Quantum tetrachotomous states: Superposition of four coherent states on a line in phase space

Namrata Shukla,[1,*] Naeem Akhtar,[2,†] and Barry C. Sanders[1,2,3,‡]

[1]*Institute for Quantum Science and Technology, University of Calgary, Calgary, Alberta, Canada T2N 1N4*

[2]*Shanghai Branch, National Research Center for Physical Sciences at Microscale, University of Science and Technology of China, Shanghai 201315, China*

[3]*Program in Quantum Information Science, Canadian Institute for Advanced Research, Toronto, Ontario, Canada M5G 1M1*

(Received 8 October 2018; published 10 June 2019)

The well-studied quantum optical Schrödinger cat state is a superposition of two distinguishable states, with quantum coherence between these macroscopically distinguishable states being of foundational and, in the context of quantum-information processing, practical use. We refer to these quantum-optical cat states as quantum dichotomous states, reflecting that the state is a superposition of two options, and we introduce the term quantum multichotomous state to refer to a superposition of multiple macroscopically distinguishable options. For a single degree of freedom, such as position, we construct the quantum multichotomous states as a superposition of Gaussian states on the position line in phase space. Using this nomenclature, a quantum tetrachotomous state (QTS) is a coherent superposition of four macroscopically distinguishable states. We define, analyze, and show how to create such states, and our focus on the QTSs is due to their exhibition of much richer phenomena than for the quantum dichotomous states. Our characterization of the QTS involves the Wigner function, its marginal distributions, and the photon-number distribution, and we discuss the QTS's approximate realization in a multiple-coupled-well system.

DOI: 10.1103/PhysRevA.99.063813

I. INTRODUCTION

Schrödinger's original quantum-cat paradox arose from the puzzle that quantum mechanics has enormous ramifications on dichotomous states such as life and death for a cat [1], and this notion morphed into the simplified problem of a superposition of two macroscopically distinguishable (i.e., negligibly overlapping) coherent states, each representing a classical distinct choice. Schrödinger's coherent state $|\alpha\rangle$ is essentially a nonspreading wave-packet solution of the quadratic harmonic-oscillator potential [2] and also defined as the eigenstate of the annihilation operator $\hat{a}$,

$$\hat{a}\,|\alpha\rangle = \alpha\,|\alpha\rangle\,, \quad \alpha \in \mathbb{C}, \tag{1}$$

and the position distribution

$$\langle q|\alpha\rangle = \frac{e^{-[q-\sqrt{2}\,\mathrm{Re}(\alpha)]^2/2+iq\sqrt{2}\,\mathrm{Im}(\alpha)}}{\pi^{1/4}}. \tag{2}$$

Milburn first showed the Q function (Husimi distribution [3]) for this so-called cat state but did not discuss it explicitly [4].

Yurke and Stoler explicitly studied this fascinating superposition state [5] via the position distribution

$$\mathrm{pr}(q) = |\langle q|\psi\rangle|^2, \quad \psi(q) \in L^2(\mathbb{R}), \quad q \in \mathbb{R}, \tag{3}$$

and the momentum distribution

$$\tilde{\mathrm{pr}}(p) = |\langle q|\tilde{\psi}\rangle|^2, \quad \tilde{\psi}(p) = \int_{\mathbb{R}} dq\,\psi(q)\,e^{iqp},$$
$$p \in \mathbb{R},\ \hbar \equiv 1. \tag{4}$$

These canonical-variable distributions (3) and (4) are obtained from the Wigner function [6–9]

$$W(q,p) = \frac{1}{2\pi}\int_{\mathbb{R}} dx\,e^{ipx}\psi^*\left(q+\frac{x}{2}\right)\psi\left(q-\frac{x}{2}\right) \tag{5}$$

as marginal distributions [9]

$$\mathrm{pr}(q) = \int_{\mathbb{R}} dp\,W(q,p), \quad \tilde{\mathrm{pr}}(p) = \int_{\mathbb{R}} dq\,W(q,p), \tag{6}$$

with these properties (6) being strong motivation for representing states by Wigner functions. Wigner functions have been used to study superpositions of Gaussian states [10,11].

The study by Milburn [4], its elaboration and extension by Milburn and Holmes [12], and its study in the context of quantum-optical cat states by Yurke and Stoler [5] all focused on superpositions of Gaussian states

$$\vartheta(q;\mu,\sigma) = e^{iq\sqrt{2}\,\mathrm{Im}(\alpha)}\sqrt{G(q;\mu,\sigma)} \tag{7}$$

and

$$G(q;\mu,\sigma) := \frac{1}{\sqrt{2\pi}\sigma}\exp\left\{-\frac{1}{2}\left(\frac{q-\mu}{\sigma}\right)^2\right\}, \tag{8}$$

with position distribution

$$|\vartheta(q;\mu,\sigma)|^2 = G(q;\mu,\sigma). \tag{9}$$

In the special case of coherent states [13],

$$\left\{|\alpha\rangle\,;\alpha \in \mathbb{C}, \alpha(q) = \vartheta\left(q;\sqrt{2}\mathrm{Re}(\alpha),\frac{1}{\sqrt{2}}\right)\right\}. \tag{10}$$

*namrata.shukla1@ucalgary.ca
†naeemakhtar@mail.ustc.edu.cn
‡sandersb@ucalgary.ca

In the Fock-state basis $\{|n\rangle\,; n \in \mathbb{N}\}$, the coherent state is

$$|\alpha\rangle = e^{-|\alpha|^2/2} \sum_{n=0}^{\infty} \frac{\alpha^n}{\sqrt{n!}} |n\rangle\,, \tag{11}$$

leading to the Poisson-number distribution

$$\wp_{\rm cs}(n;\alpha) := e^{-|\alpha|^2} \frac{|\alpha|^{2n}}{n!} \tag{12}$$

with mean

$$\langle n\rangle = |\alpha|^2 \tag{13}$$

and variance

$$\langle (n - \langle n\rangle)^2\rangle = |\alpha|^2 \tag{14}$$

equal to each other both.

In quantum optics, the Schrödinger cat state typically refers to the (unnormalized) superposition of coherent states

$$|\alpha\rangle + e^{i\varphi}\,|-\alpha\rangle\,. \tag{15}$$

The cases of $\varphi = 0$ and $\varphi = \pi$ are known as the even and odd coherent states, respectively [14], and $\varphi = \pi/2$ corresponds to the case that the cat state has a Poissonian photon-number distribution [5]. Variants have been studied such as superpositions of squeezed states [15], which are essentially the full gamut of Gaussian states (7), phase states [16], significantly overlapping coherent states (hence only partially distinguishable and known as kitten states) [17,18], multimode coherent states also known as entangled coherent states [19–22], and superpositions generalizing coherent states from rank-1 SU(2) and SU(1,1) symmetries [23] to higher-rank groups such as SU(3) [24].

Almost all studies of coherent-state superpositions stay true to the essence of Schrödinger's life-death dichotomy, but a few studies ventured into quantum multichotomous states. Superpositions of coherent states on the circle [25–27], with applications such as showing the limit yields a coherent-state representation of the Fock number state on the circle [28], form one branch of studies of superpositions of multiple coherent states.

Another investigative branch of superpositions of multiple coherent states corresponds to the superposition of Gaussian states, e.g., superpositions of coherent states and superpositions of squeezed states, on the real line in phase space [29]. Such states can be studied as an unnormalizable superposition of an infinite number of equally spaced coherent states represented in phase space, which we refer to as a comb state [29] (and here we refer to comb states with a finite number of peaks, or teeth, also as comb states with the context making clear whether an infinite or a finite number of teeth is implied), also studied under realistic limitations [30] and experimentally realized with a single trapped-ion mechanical oscillator [31]. A particular case of superpositions of coherent states on the line in phase space, which we call a quantum tetrachotomous state (QTS), as well as superpositions of a continuum of coherent states (10), was studied for the squeezing properties [25,32,33]. Zurek [34] showed that a superposition of equispaced coherent states on the circle, called a compass state, exhibits sub-Planck structure in phase space with intriguing ramifications for decoherence. Zurek's result differs from ours in being a superposition of coherent states that are not on a line in phase space but does reinforce our message that a superposition of coherent states can yield rich phenomena.

Here we study QTSs as special cases of quantum multichotomous states yet capturing the rich phenomena present in such states but being sufficiently simple to capture the richness of such states. Henceforth, we write the QTS as the state $|\Upsilon\rangle$ and its position representation as

$$\Upsilon(q) = \langle q|\Upsilon\rangle. \tag{16}$$

As we expect that the QTS features will be sensitive to separation of coherent-state amplitudes in phase space, we focus on three exemplary cases of the QTSs.

These three cases are symmetric about $x = 0$, i.e.,

$$\Upsilon(q) = \Upsilon(-q). \tag{17}$$

This symmetry simplifies the expressions and readily displays the intriguing features. Furthermore, we restrict the QTS to a superposition of coherent states (10) as this simplification is common, but not universal, for quantum-optical cat states.

We treat three cases of the QTSs as a superposition of two doublets, where we use the term doublet to refer to a superposition of a pair of coherent states.

Case Υ1. The first QTS case is a superposition of two doublets, i.e., two coherent states whose amplitudes are close together in phase space (kitten state [17,18]) whereas each of the two (kitten) doublets is macroscopically distinguishable from the other (kitten) doublet.

Case Υ2. In the second case, each of the two doublets is macroscopically distinguishable, but the two doublets are close in phase space, i.e., only microscopically distinguishable.

Case Υ3. The third case corresponds to equal separation between coherent states on the line, which looks like a four-tooth comb state in the phase-space representation.

Our approach to characterizing QTSs employs Wigner functions [10], canonical position measurements [35], and photon-number distributions [8], given by

$$\wp_{\rm QTS}(n;\alpha,\beta) = |\langle n|\Upsilon\rangle|^2 \tag{18}$$

for a QTS with $|n\rangle$ the Fock state with n photons. We employ the Wigner function to analyze QTSs because the Wigner function gives meaning to talking about states as being in phase space, i.e., the phase-space representation. Essentially, the QTS $|\Upsilon\rangle$ should appear, in the Wigner-function representation, as a sum of displaced Gaussian distributions plus additional features that reveal quantum effects such as interference due to coherence between Gaussian states.

Notably, negativity of the Wigner function signifies quantum effects [36], and marginal distributions of the Wigner function directly yield a canonical position distribution arising as asymptotic limits of homodyne detection for strong local-oscillator fields [37–39]. The photon-number distribution is interesting as phase-space interference can lead to oscillations in the photon-number distribution [40], which has been studied for general quantum-optical cat states [25,41,42] including for entangled coherent states [43,44].

Various concepts for realizing quantum-optical cat states can be extended to QTSs. Caldeira and Leggett studied tunneling in a dissipative system with superconductors as the medium [45], and a catlike state can be achieved at half the

tunneling time between the two wells. Essentially, a catlike state is approximated by the ground state (GS) of a double-well potential. A QTS could arise as the GS of a multiple-coupled-well potential, as we show in this work. One way to realize the GS of a multiple-coupled-well potential can be considered as the GS of coupled Bose-Einstein condensates as a generalization of Bose-Einstein condensates in a double-well potential [46–48]. Recent advances to these concepts include generating cat states in Bose-Einstein condensates [49] and tunneling in a dissipative system realized in a superconducting medium [50].

Our paper is organized as follows. In Sec. II we present background for quantum-optical cat states including characterization using Wigner functions, canonical marginal distributions, and photon-number distributions. Our background section also includes the realization of quantum-optical cat states as an approximate GS of a double-well potential plus experimental generation of quantum-optical cat states. In Sec. III we describe our approach to analyzing the QTS. Analysis and results appear in Sec. IV, Sec. V contains a discussion, and Sec. VI summarizes.

II. BACKGROUND

In this section we discuss the theory of quantum-optical cat states, characterizations of such states, and their experimental creation. Furthermore, we present the analogy between quantum-optical cat states with the GS of a double-well potential.

A. Theory

In this section we present the theory for characterization of quantum-optical cat states involving the Wigner function. Additionally, we discuss the marginal distribution and the inverse radon transform in this context.

The quantum-optical cat state has been characterized using various quasiprobability distributions [3,13,51,52] that are advantageous because they can be compared to classical systems represented in phase space. The Wigner function is now a typical tool for studying quantum-optical cat states and their interference pattern [11,25]. Cat states are typically characterized by performing rotated position quadrature measurements [35] or, in quantum-optics language, homodyne measurements from which the Wigner function can be constructed via, e.g., the inverse radon transform [9].

Depending on the separation between coherent states $|\pm\alpha\rangle$, which is given by the distance $2|\alpha|$ in phase space, their superpositions are referred as a quantum-optical cat state or as a kitten state for large or small interstate separation compared to the width of the coherent state. The Wigner function for this superposition is

$$\begin{aligned} W_{\rm cs}(q,p;\alpha) &= \frac{1}{2\pi}\int_{\mathbb{R}} dx\, e^{ipx}\left\langle q-\frac{x}{2}\middle|\alpha\right\rangle\left\langle\alpha\middle|q+\frac{x}{2}\right\rangle \\ &= \frac{1}{\sqrt{2}\pi}e^{-p^2/2-2(q+\alpha)^2} \\ &= \frac{1}{\sqrt{2}}G(p;0,1)G\left(q;-\alpha,\frac{1}{2}\right) \end{aligned} \tag{19}$$

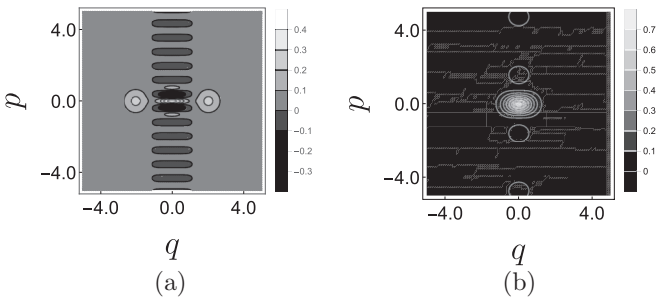

FIG. 1. Wigner function for $|\alpha\rangle + |-\alpha\rangle$ with (a) $\alpha = 2$ (cat state) and (b) $\alpha = 0.5$ (kitten state). The quantities are in arbitrary units.

with Gaussian distribution G [Eq. (8)]. Contours of the Wigner functions for even and odd quantum-optical cat states are shown in Fig. 1. Yurke and Stoler [5] used the marginal distributions as canonical phase-space-rotated position and momentum distributions when they first explained the quantum-optical cat states. The Wigner function for a quantum-optical cat state is

$$\begin{aligned} &W_{\rm cat}(q,p;\alpha) \\ &\quad= \frac{1}{2\pi N_\alpha}\int_{\mathbb{R}} dx\, e^{ipx}\left[\left\langle q-\frac{x}{2}\middle|\alpha\right\rangle+\left\langle q-\frac{x}{2}\middle|-\alpha\right\rangle\right] \\ &\qquad\times\left[\left\langle\alpha\middle|q+\frac{x}{2}\right\rangle+\left\langle-\alpha\middle|q+\frac{x}{2}\right\rangle\right], \end{aligned} \tag{20}$$

which is simplified to

$$\begin{aligned} W_{\rm cat}(q,p;\alpha) =& \frac{e^{-p^2/2}}{\sqrt{2}\pi N_\alpha}\Bigg[e^{-2(q+\alpha)^2}+e^{-2(q-\alpha)^2} \\ &+\underbrace{e^{-2q^2-2ip\alpha}+e^{-2q^2+2ip\alpha}}_{2e^{-2q^2}\cos 2p\alpha}\Bigg] \end{aligned} \tag{21}$$

for normalization

$$N_\alpha = 2(1+e^{-2\alpha^2}) \tag{22}$$

for real-valued even coherent state $|\alpha\rangle + |-\alpha\rangle$. Using the Gaussian-distribution notation (8) and introducing

$$G_+(x;\gamma,\sigma) := G(x;\gamma,\sigma) + G(x;-\gamma,\sigma), \tag{23}$$

the Wigner function for the quantum-optical cat state is

$$\begin{aligned} W_{\rm cat}(q,p;\alpha) = \frac{1}{\sqrt{2}N_\alpha}\Bigg[&G(p;0,1)G_+\left(q;\alpha,\frac{1}{2}\right) \\ &+e^{-2\alpha^2}G\left(q;\alpha,\frac{1}{2}\right)G_+(p;2i\alpha,1)\Bigg]. \end{aligned} \tag{24}$$

The first two terms in Eq. (24) are the Gaussian distributions corresponding to the coherent states and the last two terms are responsible for the interference pattern between these two coherent states in the phase space. The interference pattern can be explained by the periodic oscillatory functions appearing as coefficients to the Gaussians.

B. Quantum-state tomography and marginal distributions

For quantum-state tomography, marginal distributions for the Wigner function can be used to estimate the Wigner

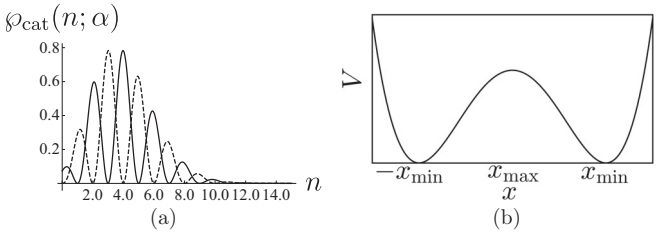

FIG. 2. (a) Photon-number distribution ($\alpha = 2$) for even coherent state $|\alpha\rangle + |-\alpha\rangle$ (solid line) and odd coherent state $|\alpha\rangle - |-\alpha\rangle$ (dashed line). (b) Potential energy as a function of position x with local minima $\pm x_{\rm min}$ and local maximum $x_{\rm max}$. The quantities are in arbitrary units.

function via the inverse radon transformation [9]. Operationally, a series of homodyne measurements, obtained for many choices of local-oscillator phase, yields data that are then inserted into an algorithm that calculates an approximation to the state's Wigner function.

The position and momentum marginal distributions for the quantum-optical cat state are

$$\mathrm{pr}_{\rm cat}(q) = \frac{1}{N_\alpha} G_+^2\left(q;\alpha,\frac{1}{\sqrt{2}}\right) \tag{25}$$

and

$$\widetilde{\mathrm{pr}}_{\rm cat}(p) = \frac{2\sqrt{2}}{N_\alpha} G(p;0,1)\cos^2 p\alpha, \tag{26}$$

which are a mixture of two Gaussians and a sinusoidally modulated Gaussian, respectively.

C. Interference in phase space

The photon-number distribution for a general superposition of coherent states reveals interference in phase space [25,41]. This interference effect arises from the term that is sensitive to the relative phase difference between superposed coherent states. The photon-number distribution for an even (+) and an odd (−) cat state (15) is

$$\wp_{\rm cat}(n;\alpha) \propto [1 \pm (-1)^n]\wp_{\rm cs}(n;\alpha), \tag{27}$$

with $\wp$ the Poisson distribution (12). This Poisson distribution is shown in Fig. 2. Due to interference, even coherent states exhibit only an even number of photons. For the odd coherent states, we observe only odd numbers of photons [40,44]. The photon-number distribution is modulated by interference between the two coherent states in the superposition.

Oscillations in the photon-number distribution are due to interference in phase space [8,40], and this kind of oscillation (27) has been studied for superpositions of coherent states on a line and superposition of coherent states on a circle in phase space [27]. The closer the coherent states are to each other, the less distinguishable the peaks are from the interference fringes as shown in Fig. 1(b). As the separation between the Gaussian peaks on the phase-space position line decreases to the point that the interferences fringes and peaks lose distinguishability, momentum squeezing becomes evident.

D. Generating quantum-optical cat states

The original proposals for generating optical cat states (15) were achieved via nonlinear interactions [53–56] subsequently followed by proposals for manipulating photons in a cavity by dispersive atom-field coupling [57]. Generating quantum-optical cat states by photon subtraction is an appealing approach [58,59]. An approximation to quantum-optical Schrödinger kitten states can be prepared with a squeezed-light resource [17], and a squeezed Schrödinger cat state has been approximately created using homodyne detection and photon-number states as resources [18].

Cat states could be created by two interacting Bose condensates [47]. Alternatively, cat states could be realized with two trapped, coupled Bose-Einstein condensates with a Josephson coupling [46]. One enticing method to create a quantum-optical cat state, i.e., a quantum dichotomous state (QDS), is via constructing a GS of a coherently coupled Bose-Einstein condensate in a double-well potential by means of scattering light and quantum measurement [48]. We discuss the double-well potential next.

E. Double-well potential

In this section we discuss the coherent state as the GS of a quadratic potential and its extension to a QDS as the GS of a double-well potential. Quantum tunneling is valuable for many applications, with one foundational example being the case studied by Caldeira and Leggett to ascertain how long range quantum coherence can be [45,60].

A superposition of coherent states (15) can be created for large amplitudes $|\alpha| \gg 1$ using the motional state of a trapped ion in an approximate harmonic-oscillator potential using ultrafast laser pulses and coupling a qubit with a harmonic oscillator [61–65]; some of these methods can be extended to multicomponent superpositions of coherent states such as the QTS [62,64]. This superposition of coherent states can also be constructed as the GS of a coherently coupled Bose-Einstein condensate in a double-well potential [46,47] or the evolution of a Bose-Einstein condensate in a double-well potential in a two-mode approximation [48]. In the latter case, macroscopic quantum coherence of Bose-Einstein condensates leads to coherent quantum tunneling of atoms between the two modes representing two Bose-Einstein condensates, thereby creating a QDS.

Other experimental proposals include conditional generation of QDSs [66–72] with applicability to quantum-information processing [73–75]. Creation of QDSs, with the crucial macroscopic separation required to observe the quantum effects, is thus based on some degree of approximation such as the method proposed by Caldeira and Leggett [45].

Schrödinger showed that coherent states follow the motion of a classical particle in a quadratic potential [1,76] and the GS is a coherent state with zero mean amplitude. For a double-well system, coupling two nearly harmonic oscillators together via a finite barrier, which is approximated by an inverted harmonic oscillator in the vicinity of the unstable maximum potential between the two wells, the localized GS in each well can be approximated by a coherent state (10), with mean amplitude corresponding to the displacement of the well from the origin of phase space. The harmonic-oscillator

assumptions for the minima and maximum (inverted harmonic potential in that case) are quite good for analytic potentials due to convergence of the Taylor series around minima and maxima. The minima are stable points with zero-motion solutions classically and the maximum is a turning point classically. In the rest of the paper we refer to stable and unstable points in phase space and their respective localized states in those regions.

Nandi [77] has proposed a way of creating a double-well potential by multiplying the Gaussian (8) by a factor of x^2. This potential function, which is essentially a second-order Hermite-Gaussian function with a pure Gaussian subtracted, is symmetric about $x = 0$. In this way, the Hamiltonian can be brought into a symmetric tridiagonal form. This system has been numerically solved to study the energy levels. The tunneling rate of the particle in such a potential well depends on the energy difference between the ground and the first excited state. The higher or wider the barrier the smaller this energy difference and this difference will become larger as the energy of the incident particle increases.

Equipped with this background and the limitations to construct and characterize a Schrödinger cat state (QDS), we now develop our concept of the QTS. The QTS as we define in the next section is in some sense a superposition of two QDSs. In the next section we also discuss the tools and methods to analyze QTSs and study their appearance and behavior in the phase space.

III. APPROACH

In this section we describe our approach to analyzing QTSs. Our approach involves characterization by the Wigner function, the marginal distribution, and the approximate realization of the QTSs via a multiple-coupled-well system, i.e., quadrupole-Gaussian-well potential. We also study the photon-number distribution of the QTS and observe the oscillatory behavior due to the four-level interference patterns between the coherent states.

A. Defining the tetrachotomous cat

In this section we define the QTS along similar lines to idea of the QDS. We also discuss how the QTS can be in three different configurations depending on the superposition between the coherent states forming QDSs and the overlap between two such QDSs. This section also includes the symmetry transformations of the constituent coherent states and how they change the QTS. We define the QTS by extending the concept of QDSs by splitting its two states into two distinguishable states each. The QTS can be thought of as the superposition of two coherent states separated macroscopically, each consisting of two coherent states with opposite phases and distinguishable. The even QTS is

$$|\Upsilon\rangle \propto |\alpha\rangle + |-\alpha\rangle + |\beta\rangle + |-\beta\rangle \tag{28}$$

and the odd QTS is

$$|\Upsilon\rangle_{\rm odd} \propto |\alpha\rangle - |-\alpha\rangle - |\beta\rangle - |-\beta\rangle\,, \tag{29}$$

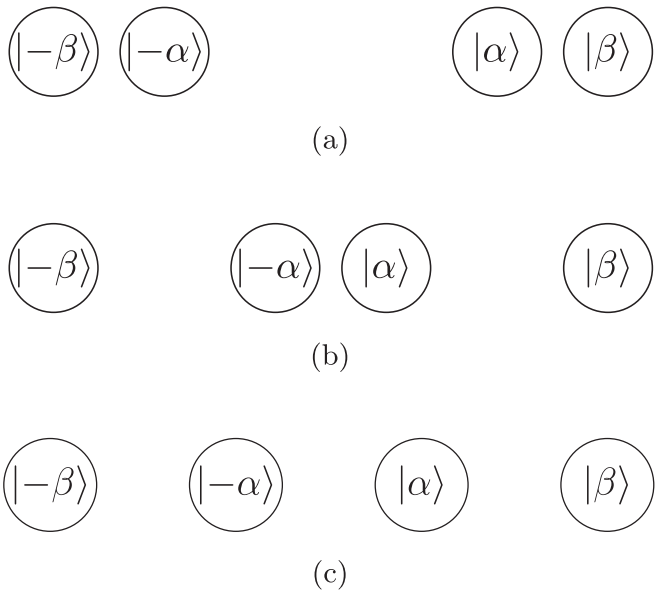

FIG. 3. Illustrative phase-space picture of the linear QTSs (28) and (29) for (a) case 1, (b) case 2, and (c) case 3.

up to a normalization factor. We study only even QTSs (28) as the symmetry

$$\alpha \leftrightarrow \beta, \quad \alpha \leftrightarrow -\alpha, \quad \beta \leftrightarrow -\beta, \quad \alpha \leftrightarrow -\beta, \quad \alpha \leftrightarrow \beta \tag{30}$$

keeps the state the same, making analysis straightforward, and we do not lose generality in how to study QTSs. We consider three different types of QTS (28) enumerated as cases $\Upsilon1$–$\Upsilon3$ in Sec. I. For case $\Upsilon1$, we have a superposition of two macroscopically separated kitten doublets [Fig. 3(a)]. The second case $\Upsilon2$ is a superposition of two macroscopically distinguishable doublets but with the two doublets somewhat overlapping [Fig. 3(b)]. The third case $\Upsilon3$ is four equally spaced coherent states on the real line in phase space [Fig. 3(c)].

B. Wigner function and marginal distributions

In this section we describe the Wigner function and marginal distributions for studying the phase-space properties of the QTSs. In terms of Gaussian functions (8), the QTS (28) Wigner function $W_{\rm QTS}(q, p)$ satisfies

$$\begin{aligned} &W_{\rm QTS}(q, p; \alpha, \beta) \\ &= \frac{1}{\sqrt{2}N_{\alpha,\beta}}\left\{G(p;0,1)\left[G_+\left(q;\alpha,\frac{1}{2}\right)+G_+\left(q;\beta,\frac{1}{2}\right)\right]\right. \\ &\quad + G\left(q;0,\frac{1}{2}\right)[e^{-2\alpha^2}G_+(p;2i\alpha,1)+e^{-2\beta^2}G_+(p;2i\beta,1)] \\ &\quad + e^{-(\alpha-\beta)^2}\left[G_+\left(q;\frac{\alpha+\beta}{2},\frac{1}{2}\right)G_+(p;i(\alpha-\beta),1)\right] \\ &\quad \left.+ e^{-(\alpha+\beta)^2}\left[G_+\left(q;\frac{\alpha-\beta}{2},\frac{1}{2}\right)G_+(p;i(\alpha+\beta),1)\right]\right\} \end{aligned} \tag{31}$$

for normalization

$$N_{\alpha,\beta} = 2(1+e^{-2\alpha^2}) + 2(1+e^{-2\beta^2}) + 4(e^{-(\alpha-\beta)^2/2} + e^{-(\alpha+\beta)^2/2}). \tag{32}$$

This compact notation G and $G_\pm$ in Eq. (31) greatly simplifies the Wigner-function expression and makes interpretation of complicated plots relatively easy. Now we explain the terms in this complicated expression.

The first term in Eq. (31) represents the four Gaussians located at $\pm\alpha$ and $\pm\beta$ on the phase-space position axis, corresponding to four coherent states. The second term in (31) represents the interference terms between the doublets at $|\pm\alpha\rangle$ and $|\pm\beta\rangle$. The third term in (31) corresponds to interference between the pair $|\alpha\rangle$ and $|\beta\rangle$ and the pair $|-\alpha\rangle$ and $|-\beta\rangle$. The last term (31) shows interference between the pair $|\alpha\rangle$ and $|-\beta\rangle$ and the pair $|-\alpha\rangle$ and $|\beta\rangle$.

Expression (31) readily shows that the interference between each pair of real-amplitude coherent states $|\pm\alpha\rangle$ and $|\pm\beta\rangle$, which is symmetric about zero on the phase-space position axis, is located at the center of the position axis. However, interference between the pairs $\{|\alpha\rangle, |\beta\rangle\}$ and $\{|-\alpha\rangle, |-\beta\rangle\}$ is centered at $\pm\frac{\alpha+\beta}{2}$ and similarly the interference between $\{|\alpha\rangle, |-\beta\rangle\}$ and $\{|-\alpha\rangle, |\beta\rangle\}$ is centered at $\pm\frac{\alpha-\beta}{2}$, respectively. Functions of the type $G(p; i\alpha, \sigma)$ are Gaussian-modulated sinusoidal oscillations along the momentum coordinate of phase space and represent interference between the coherent states in the QTS. The QTS marginal distributions obtained from the Wigner function following Eq. (6) are

$$\mathrm{pr}_{\mathrm{QTS}}(q) = \frac{1}{N_{\alpha,\beta}}\left[G_+\left(q;\alpha,\frac{1}{\sqrt{2}}\right) + G_+\left(q;\beta,\frac{1}{\sqrt{2}}\right)\right]^2 \tag{33}$$

for position and

$$\widetilde{\mathrm{pr}}_{\mathrm{QTS}}(p) = \frac{2\sqrt{2}}{N_{\alpha,\beta}}[G(p;0,1)(\cos p\alpha + \cos p\beta)^2] \tag{34}$$

for momentum. Equations (33) and (34) can be compared to Eqs. (25) and (26) for the QDS; evidently, the marginal distribution for the QTS along the position axis has four Gaussian peaks whereas the QDS has two Gaussian peaks and the marginal distribution along the momentum axis for QTS has an interference pattern as a Gaussian modulated by

$$(\cos p\alpha + \cos p\beta)^2, \tag{35}$$

which looks like a Cartesian lattice of mountains over $\mathbb{R}^2$ with coordinates α and β. For the QDS marginal distribution, the appearance of the function (35) as a beat between two tones explains observed interference.

C. Photon-number distribution

The photon-number distribution for the QTS is applied for the three cases $\Upsilon1$–$\Upsilon3$ explained in Sec. III A. As an extension of QDSs, photon-number distributions for QTSs are Poissonian distributions corresponding to two QDSs, each of them with an oscillatory nature. Peaks of the oscillation in photon-number distributions are centered at even photon numbers for even QTSs and at odd photon numbers for odd QTSs as evident in

$$\wp^{\pm}_{\mathrm{QTS}}(n;\alpha,\beta) = [1\pm(-1)^n]\tilde{\wp}_{\mathrm{QTS}}(n;\alpha,\beta) \tag{36}$$

for

$$\tilde{\wp}_{\mathrm{QTS}}(n;\alpha,\beta) := \frac{4}{N_{\alpha,\beta}}[\tilde{\wp}_{\mathrm{cs}}(n;\alpha,\beta) + e^{-(\alpha+\beta)^2/2+\alpha^2\beta^2}\wp_{\mathrm{cs}}(n;\alpha\beta)] \tag{37}$$

and

$$\tilde{\wp}_{\mathrm{cs}}(n;\alpha,\beta) := \frac{\wp_{\mathrm{cs}}(n;\alpha)+\wp_{\mathrm{cs}}(n;\beta)}{2}, \tag{38}$$

with $\wp_{\mathrm{cs}}(n;\alpha)$ defined in Eq. (12). As we consider only the case of an even QTS, here we only deal with $\wp^{+}_{\mathrm{QTS}}$ and henceforth drop the superscript $+$. To analyze inter-Poissonian interference we use the expression

$$\wp^{\mathrm{IP}}_{\mathrm{QTS}}(n;\alpha,\beta) = \frac{4}{N_{\alpha,\beta}}[1\pm(-1)^n]e^{-(\alpha+\beta)^2/2+\alpha^2\beta^2}\wp_{\mathrm{cs}}(n;\alpha\beta), \tag{39}$$

with the superscript $+$ suppressed and the superscript IP referring to inter-Poissonian.

The first two terms in (36) indicate that the two Poissonian curves for each QDS consists of two coherent states with the same amplitude but opposite phases, e.g., $|\pm\alpha\rangle$ and $|\pm\beta\rangle$ are peaked at $|\alpha|^2$ and $|\beta|^2$, respectively. The third term on the right-hand side of Eq. (36) represents a small interference pattern between these two Poissonian distributions.

The inter-Poissonian interference term leading is intriguing and needs to be established as interference between distinct Poissonian sectors or not. To understand the inter-Poissonian interference term, we analyze the photon-number distribution involving only the inter-Poissonian interference term in Eq. (36). To elucidate the interference effect, we take the derivative of the envelope photon-number distribution with respect to photon number n by treating n as a continuous quantity, hence using the relation $n! = \Gamma(n+1)$.

The photon-number distribution (36) has an envelope function (37), which is the sum of Poissonian distributions (38) plus the second term on the right-hand side of Eq. (37) corresponding to inter-Poissonian interference. Now we take the derivatives of the envelope function including inter-Poissonian interference (37) and excluding inter-Poissonian interference (38). The derivative of the envelope function reveals the envelope function's extrema as zeros, which makes it easy to identify the extrema and especially whether the extrema change due to inter-Poissonian interference.

We take derivatives of this envelope function (37), which includes the inter-Poissonian interference

$$\tilde{\wp}'_{\mathrm{QTS}}(n;\alpha,\beta) = \frac{N^{-1}_{\alpha,\beta}}{\Gamma(n+1)}\{2e^{-(\alpha^2+\beta^2)}(\alpha^n e^{\beta^2/2}+\beta^n e^{\alpha^2/2}) \times [2(\alpha^n e^{\beta^2/2}\ln\alpha + \beta^n e^{\alpha^2/2}\ln\beta) - (\alpha^n e^{\beta^2/2}+\beta^n e^{\alpha^2/2})\Psi^{(0)}(n+1)]\}, \tag{40}$$

and the sum (38), which does not include the inter-Poissonian interference

$$\tilde{\wp}'_{\rm cs}(n;\alpha,\beta) = \frac{N_{\alpha,\beta}^{-1}}{\Gamma(n+1)}\{e^{-(\alpha^2+\beta^2)} \times [4(\alpha^{2n}e^{\beta^2}\ln\alpha + \beta^{2n}e^{\alpha^2}\ln\beta) - (\alpha^{2n}e^{\beta^2} + \beta^{2n}e^{\alpha^2})\Psi^{(0)}(n+1)]\}. \quad (41)$$

The prime signifies differentiation with respect to n and

$$\Psi^{(0)}(n) := \frac{d}{dn}\ln[\Gamma(n)] \quad (42)$$

is the digamma function.

D. Multiple-well approximation

The idea of approximately realizing a QDS as a double-well GS is discussed in Sec. II E. Similarly, we propose a QTS implementation based on realizing the GS of a quadrupole-Gaussian-well potential under reasonable approximations.

We study a quadruple-Gaussian-potential-well structure

$$V(x) = V_{\rm g}(x-\alpha) + V_{\rm g}(x+\alpha) + V_{\rm g}(x-\beta) + V_{\rm g}(x+\beta) - V_{\rm g}(0), \quad (43)$$

where

$$V_{\rm g}(x) = -V_0\exp\left(-\frac{\gamma x^2}{2\sigma^2}\right) \quad (44)$$

is a single-well Gaussian potential centered at $x = 0$. The GS of the single-particle Hamiltonian with potential (43) serves as an approximation to the QTS. Our multiple-well potential (43) differs from Nandi's approach to creating a double-Gaussian-well potential [77], as discussed in Sec. II E, as Nandi effectively uses a Hermite-Gaussian potential well whereas we employ a sum of Gaussian wells with varied spacing to treat each QTS case described in Sec. III A. For numerical simulation, our Gaussian potential wells are approximated by piecewise-continuous functions.

Our method involves transforming a Schrödinger equation into a matrix equation from a differential equation by using the three-point finite-difference method. The matrix eigenvalue problem is solved numerically by using the inverse iteration method to obtain the Wigner function of a ground-state vector.

We compute the overlap between the ideal QTS and the corresponding GS, namely,

$$\langle {\rm GS}|\Upsilon\rangle = \int_{\mathbb{R}} dq \langle q|{\rm GS}\rangle^* \langle q|\Upsilon\rangle \quad (45)$$

for $|{\rm GS}\rangle$ the GS of the Gaussian quadruple well and $|\Upsilon\rangle$ the corresponding QTS with parameters chosen to deliver the closest match. To solve Eq. (45) numerically, we calculate both the QTS and the GS in the position representation but over discrete position bins. These bins extend over the full range of interest for the QTS and have sufficient resolution that the fine features are part of the overlap calculation. For this discrete position-bin representation of the QTS and GS vectors, the integral in Eq. (45) becomes a sum over all bins, namely, the dot product of the two complex state vectors, which, for our QTS and GS, are actually simply real valued.

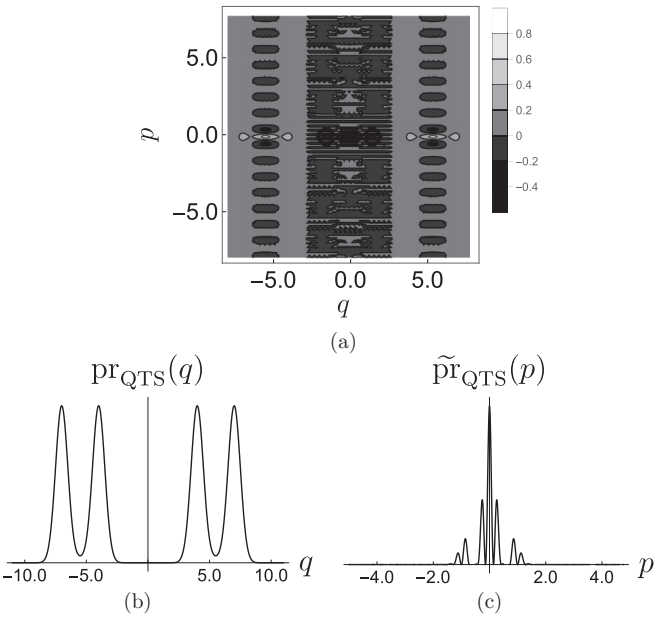

FIG. 4. (a) Wigner function, (b) position marginal distribution, and (c) momentum marginal distribution for QTS case $\Upsilon 1$ for $\alpha = 4$ and $\beta = 7$. The quantities are in arbitrary units.

IV. ANALYSIS AND RESULTS

In this section we refer to the pairs of two coherent states $|\alpha\rangle, |\beta\rangle$ and $|-\alpha\rangle, |-\beta\rangle$ as doublets and analyze three different cases of the QTS (28) based on the distinguishability between the doublet states and the states of doublets according to the three specific QTS cases: $\Upsilon 1$ with $\alpha = 4$ and $\beta = 7$ (two doublets), $\Upsilon 2$ with $\alpha = 1$ and $\beta = 6$ (doublet between two singlets), and $\Upsilon 3$ with $\alpha = 2$ and $\beta = 6$ (comb state). The first case describes the configuration in which doublets are separated by a macroscopic distance, but the coherent states forming the doublets are close. The second case describes the configuration in which two doublets are close together, but the coherent states forming the doublets are macroscopically separated. The third case is a depiction of the QTS where all the coherent states are equally spaced with macroscopic distinguishability. We apply our four tools comprising the Wigner function, marginal distributions, photon-number distribution, and finally the multiple-well approximation using the Wigner function.

A. Case $\Upsilon 1$: Two doublets

In this section we analyze the two-doublet QTS ($\Upsilon 1$). Specifically, we analyze the results for the Wigner function, the marginal distributions, the photon-number distribution, and the four-well ground-state approximation.

1. Wigner function for $\Upsilon 1$

We present the Wigner function for the $\Upsilon 1$ QTS in Fig. 4(a). In this figure we observe four Gaussian peaks in contrast to the pair of Gaussian peaks for the QDS (25) shown in Fig. 1. Whereas the QDS has a sinusoidal oscillation (26) shown in Fig. 1, the QTS has an oscillatory beat in momentum (34) shown in Fig. 4(a). For this QTS arrangement, as we

can infer from the preceding section and Eq. (31), the four flattened Gaussians located at ± 4 and at ± 7 correspond to the coherent state $|\alpha\rangle$ for $\alpha \in \{\pm 4, \pm 7\}$.

The interference patterns seen between the doublets are coming from the states $|4\rangle, |7\rangle$ and $|-7\rangle, |-4\rangle$ centered in the middle of each pair, i.e., 5.5 and -5.5, respectively. The interference at the origin is caused by $|\pm 4\rangle$ and $|\pm 7\rangle$, on its right due to the pair $|-4\rangle$ and $|7\rangle$, and on its left due to the pair $|4\rangle$ and $|-7\rangle$ centered at 1.5 and -1.5, respectively, on the position axis. The two interference patterns centered at 1.5 and -1.5 are not as distinguishable as for QDSs.

2. *Marginal distributions for* $\Upsilon 1$

The QTS marginal distributions for $\Upsilon 1$ are shown in Figs. 4(b) and 4(c) for position and momentum variables and are obtained by integrating the Wigner function over the conjugate degree of freedom. In Fig. 4(b) we see four Gaussian peaks and no interference for the marginal distribution along the position axis. However, the marginal distribution along the momentum axis in Fig. 4(c) shows an interference pattern with a Gaussian modulated by the square of the sum of two sinusoidal functions, i.e., $(\cos 4p + \cos 7p)^2$.

3. *Photon-number distribution for* $\Upsilon 1$

For the same example of $\Upsilon 1$, we plot photon-number distribution $\wp_{\rm QTS}(n;\alpha,\beta)$ [Eq. (36)] in Fig. 5(a), which shows two modulated Poissonian distributions corresponding to the two QDSs $|\pm 4\rangle$ and $|\pm 7\rangle$ with peaks located at $16 = (\pm 4)^2$ and $49 = (\pm 7)^2$ corresponding to the amplitude peaks of the QTS. The zoomed-in view of the interference effect between these two Poissonian distributions (39) is evident in Fig. 5(b). Figure 5(c) shows the derivative of the envelope photon-number distribution without the inter-Poissonian interference term given in Eq. (41). From Fig. 5(c) it is clear that the interference is too small to affect the infimum of the envelope curve in (37).

4. *Quadruple-Gaussian-well GS for* $\Upsilon 1$

We calculate the Wigner function for the approximated GS of the quadruple-Gaussian-well potential in this configuration shown in Fig. 6(a). The Wigner function for this GS is plotted in Fig. 6(b), and the pattern of the Wigner function closely matches the analytic Wigner function for this QTS configuration in Fig. 6(a). We use Eq. (45) to calculate the overlap between the GS and the QTS, which in this case is 0.9041. The close match holds in the sense that the Gaussian peaks and interference effects are at the same places in both plots for the $p = 0$ axis. Furthermore, the interference effects proceed *ad infinitum*. Minor differences between the plots are expected because the Gaussian wells only approximate parabolic potentials, which would be needed to see very close approximations to coherent states in the superposition.

B. Case $\Upsilon 2$: Doublet between two singlets

In this section we analyze the doublet-between-two-singlets QTS ($\Upsilon 2$). Specifically, we analyze the results for the Wigner function, the marginal distributions, the photon-number distribution, and the four-well ground-state approximation.

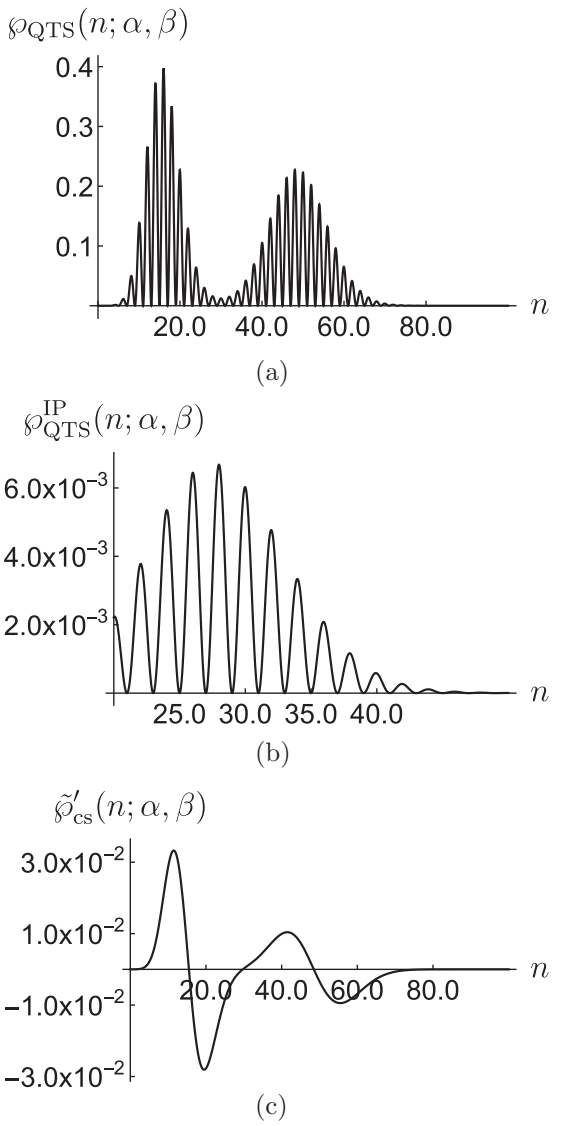

FIG. 5. For case $\Upsilon 1$, plots of (a) $\wp_{\rm QTS}(n;\alpha,\beta)$, (b) $\wp^{\rm IP}_{\rm QTS}(n;\alpha,\beta)$, and (c) $\tilde{\wp}'_{\rm cs}(n;\alpha,\beta)$ for $\alpha = 4$ and $\beta = 7$. The quantities are in arbitrary units.

1. *Wigner function for* $\Upsilon 2$

We present the Wigner function for the $\Upsilon 2$ QTS in Fig. 7(a). The locations of the Gaussians corresponding to states $|\pm 1\rangle$ and $|\pm 6\rangle$ on the position axis are ± 1 and ± 6. The interference pattern at the origin is due to the coherent states $|\pm 1\rangle$ and $|\pm 6\rangle$, but the states $|\pm 1\rangle$ are too close to form a QDS and the Gaussians corresponding to these states run into each other as in Fig. 1(b). This proximity between states represented in phase space causes the Gaussian peaks at ± 1 not showing explicitly and leading to the interference pattern between $|-6\rangle, |1\rangle$ centered at -2.5 overlap with $|-6\rangle, |-1\rangle$ at -3.5 and $|6\rangle, |-1\rangle$ at 2.5 overlap with $|6\rangle, |1\rangle$ at 3.5.

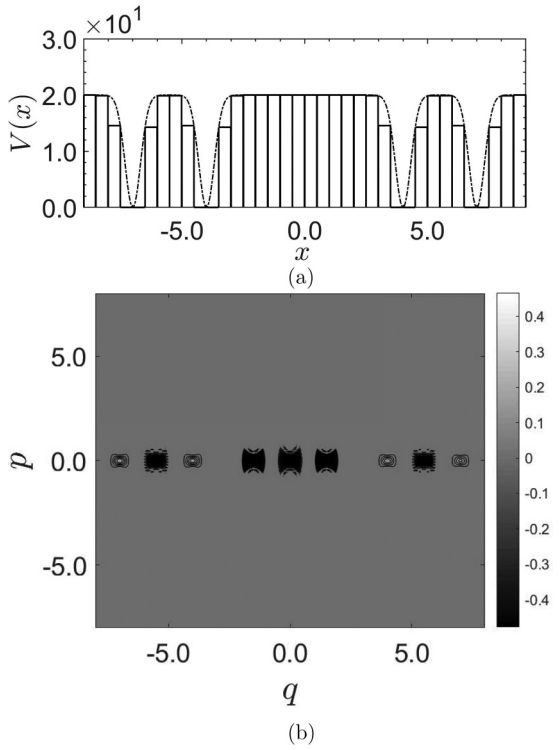

FIG. 6. For case ϒ1, (a) quadrupole-Gaussian-well potential approximated as a piecewise continuous function and (b) ground-state Wigner function for the potential $V(x)$ for $\alpha = 4$ and $\beta = 7$. The quantities are in arbitrary units.

These overlaps cause the interference patterns to spread along the q axis.

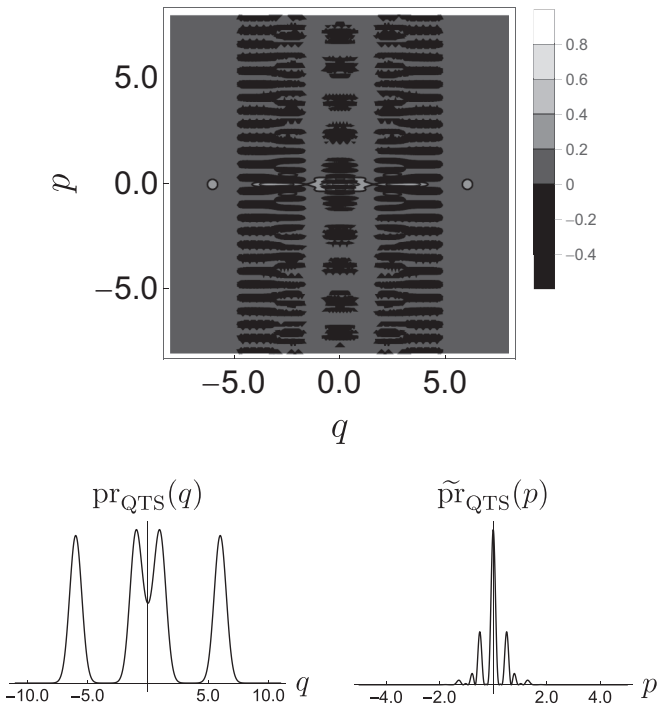

FIG. 7. (a) Wigner function, (b) position marginal distribution, and (c) momentum marginal distribution for QTS case ϒ2 for $\alpha = 1$ and $\beta = 6$. The quantities are in arbitrary units.

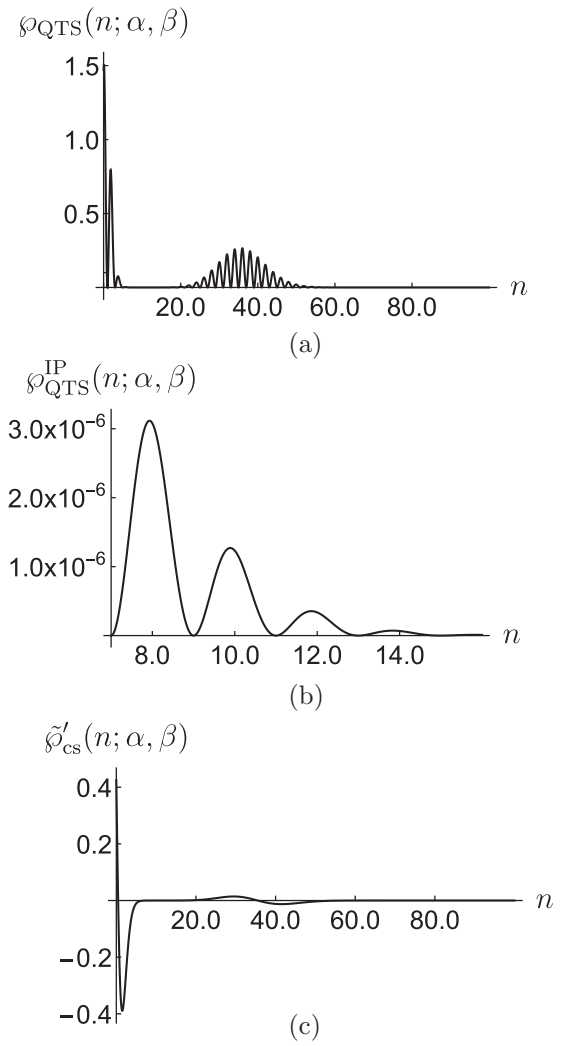

FIG. 8. For case ϒ2, plots of (a) $\wp_{\rm QTS}(n;\alpha,\beta)$, (b) $\wp^{\rm IP}_{\rm QTS}(n;\alpha,\beta)$, and (c) $\tilde{\wp}'_{\rm cs}(n;\alpha,\beta)$ for $\alpha = 1$ and $\beta = 6$. The quantities are in arbitrary units.

2. *Marginal distributions for* ϒ2

The QTS marginal distributions for configuration ϒ2 are shown in Figs. 7(b) and 7(c). We see the Gaussian peaks at ± 1 and ± 6 along the position axis and an interference Gaussian modulated by $(\cos p + \cos 6p)^2$ along the momentum quadrature.

3. *Photon-number distribution for* ϒ2

Figure 8(a) shows the photon-number distribution for this arrangement of the QTS ϒ2. The two Poissonians are peaked at 1 and 36 for the QDS $|\pm 1\rangle$ and QDS $|\pm 6\rangle$, respectively. As the separation between the QDS formed by $|\pm 1\rangle$ is small, the Poissonian curve peaked at 1 is narrow. Figure 8(b) shows the interference effect as in Eq. (39) plotted against n. It shows that the interference arising between the two QDSs $|\pm 1\rangle$ and $|\pm 6\rangle$ is the smallest among all the cases probably because the pair $|\pm 1\rangle$ does not have enough separation between them. As expected, Fig. 8(c) shows that the small inter-Poissonian interference does not change the photon-number distribution significantly at the envelope level.

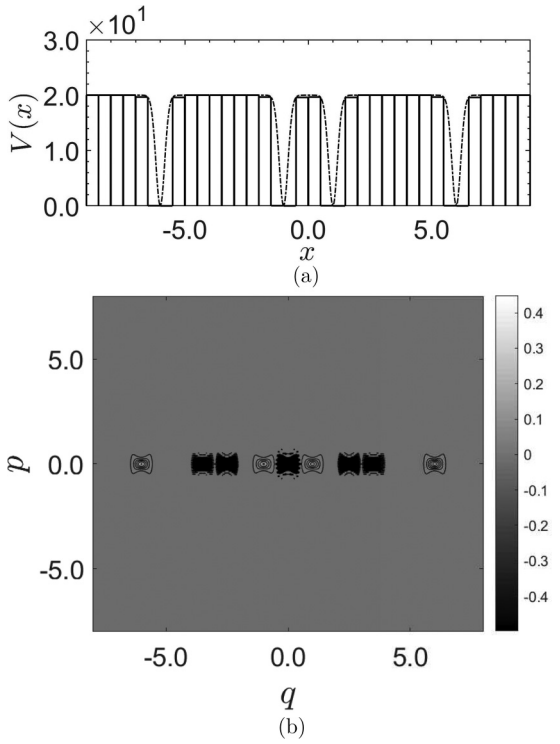

FIG. 9. For case ϒ2, (a) quadrupole-Gaussian-well potential approximated as a piecewise continuous function and (b) ground-state Wigner function for the potential $V(x)$ for $\alpha = 1$ and $\beta = 6$. The quantities are in arbitrary units.

4. *Quadruple-Gaussian-well ground state for* ϒ2

The four-well Gaussian potential for this case is depicted in Fig. 9(a). The Wigner function calculated for the approximated GS of this potential is shown in Fig. 9(b). The locations of Gaussian peaks and the centers of the interference patterns between each pair of coherent states agree with Eq. (31) and are plotted in Fig. 7(a). The numerical overlap between the GS and the QTS using Eq. (45) in this case is 0.8780.

C. Case ϒ3: Comb state

In this section we analyze the comb-state QTS (ϒ3). Specifically, we analyze the results for the Wigner function, the marginal distributions, the photon-number distribution, and the four-well ground-state approximation.

1. *Wigner function for* ϒ3

The third case as shown in Fig. 3(c) corresponds to a cat having two states, each split into doublets with the same overlap as the two doublets (ϒ3). The Wigner function for this case is depicted in Fig. 10(a) and it shows only one pair of Gaussians corresponding to $|\pm 6\rangle$ centered at ± 6 on the position axis. Whenever $3\alpha = \beta$, which is the case here, interference coincides with Gaussians peaks, resulting in a spreading of the interference pattern along the q axis.

2. *Marginal distributions for* ϒ3

The QTS marginal distributions for configuration ϒ2 are shown in Figs. 10(b) and 10(c). We see the Gaussian peaks at

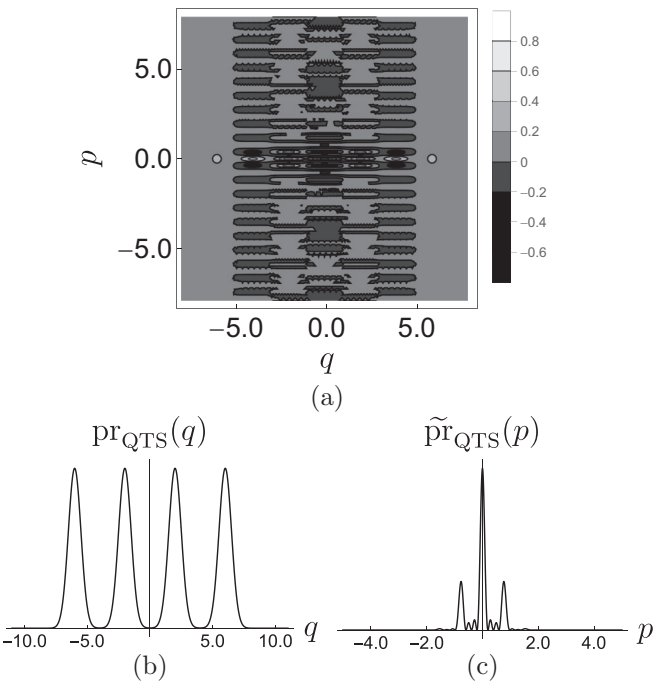

FIG. 10. (a) Wigner function, (b) position marginal distribution, and (c) momentum marginal distribution for QTS case ϒ3 for $\alpha = 2$ and $\beta = 6$. The quantities are in arbitrary units.

± 2 and ± 6 along the position axis and an interference Gaussian modulated by $(\cos 2p + \cos 6p)^2$ along the momentum quadrature.

3. *Photon-number distribution for* ϒ3

The photon-number distribution in this QTS arrangement for configuration ϒ2 appears in Fig. 11(a). Poisson distributions are clearly well separated with their highest peaks located at 4 and 36 in phase space because the QDSs $|\pm 2\rangle$ and $|\pm 6\rangle$ are well separated. A closer view of inter-Poissonian interference (39) is depicted in Fig. 11(b). Compared to previous cases, interference in this case is more pronounced than for the QTS configuration for ϒ2 but less than for ϒ1. The derivative of the envelope curve without the inter-Poissonian interference term (41) in Fig. 11(c) shows that the interference between the Poissonian distributions does not affect the maxima and minima of the photon-number distribution.

4. *Quadruple-Gaussian-well ground state for* ϒ3

The Wigner function calculated for the approximate ground state of the quadruple-Gaussian-well potential arrangement shown in Fig. 12(a) is depicted in Fig. 12(b). The Wigner-function interference patterns for this approximated GS coincide with the Wigner function that has been analytically constructed for this QTS in Fig. 10(a). The overlap using Eq. (45) in this case is 0.9313, which confirms the pattern match.

V. DISCUSSION

In this section we interpret and summarize the results for each of the three cases discussed for the four tools

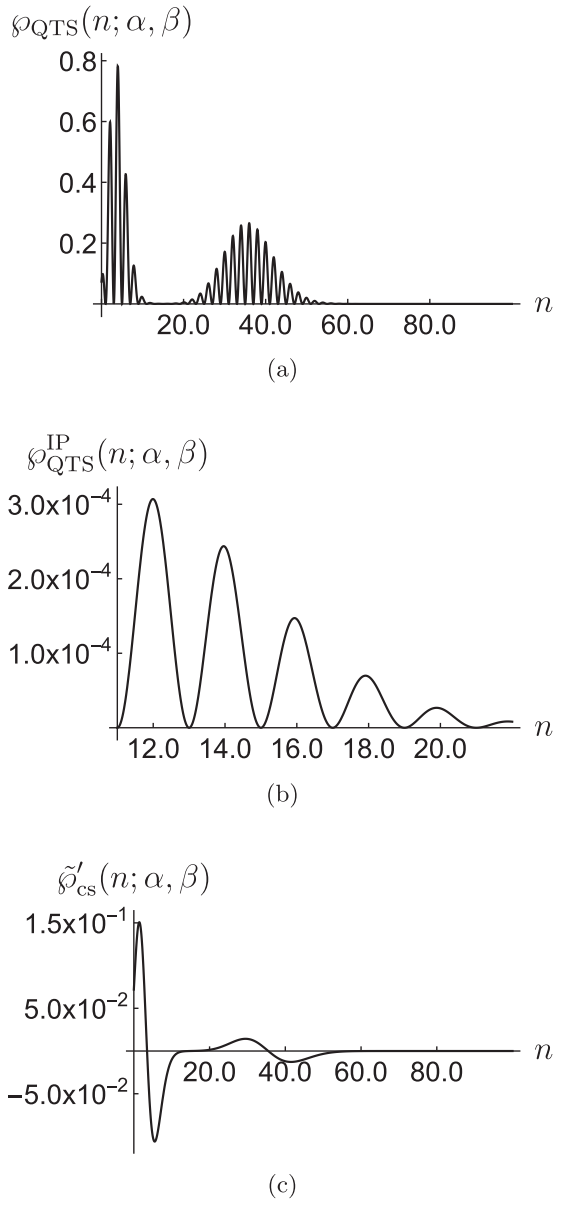

FIG. 11. For case $\Upsilon 3$, plots of (a) $\wp_{\rm QTS}(n;\alpha,\beta)$, (b) $\wp^{\rm IP}_{\rm QTS}(n;\alpha,\beta)$, and (c) $\tilde{\wp}'_{\rm cs}(n;\alpha,\beta)$ for $\alpha = 2$ and $\beta = 6$. The quantities are in arbitrary units.

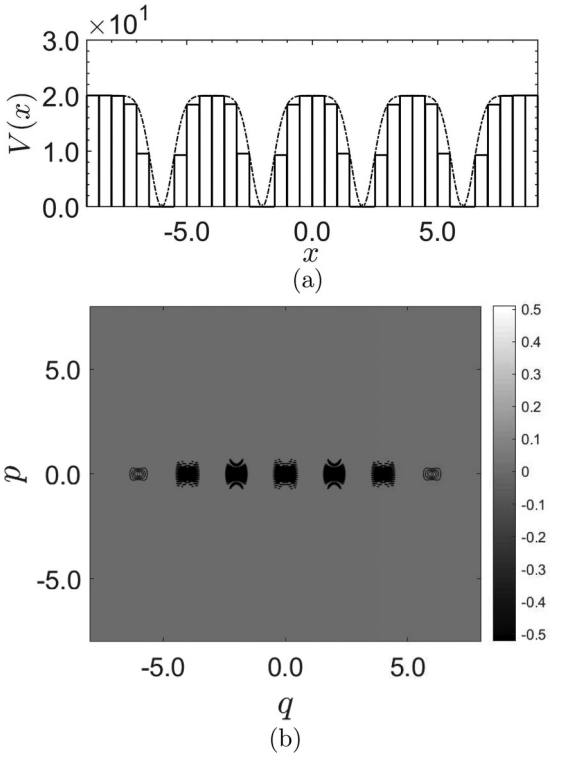

FIG. 12. For case $\Upsilon 3$, (a) quadrupole-Gaussian-well potential approximated as a piecewise continuous function and (b) ground-state Wigner function for the potential $V(x)$ for $\alpha = 2$ and $\beta = 6$ ($\Upsilon 3$). The quantities are in arbitrary units.

comprising the Wigner function, the marginal distributions, and the photon-number distribution. One intuitive result is that the Wigner function for each QTS is understood, due to linearity, as a superposition of the $\binom{4}{2} = 6$ QDS phenomena.

This insight helps to show clearly what the otherwise complicated Wigner-function patterns are showing. Interference in the Wigner function is quite evident if the QDSs are greatly separated between coherent-state components (the cat-state case) and exhibit interference poorly for small separation between coherent states (the kitten-state case). If interference coincides with a Gaussian peak, the Gaussian peak is thus diminished. This coincidence of peak and trough is important for comb states, which are equally spaced so most Gaussians peaks are colocated with strong interference troughs. Thus, the comb state displays almost vanishing Gaussians (the two in the middle of the QTS).

We remark that our comb state differs from the experimental trapped-ion grid state [31], with the grid state having an unequally weighted superposition of coherent states whereas the comb state has equal weighting. The grid state displays a Wigner-function pattern with diminished interference patterns between some pairs of coherent states probably due to this unequal weighting and probably also due to extreme sensitivity of the interference pattern on the periodicity of coherent-state amplitudes in phase space.

For marginal distributions, the Gaussian peaks are well separated and interference along the p axis is clear. For the kitten state, Gaussian peaks run together. The p distributions also show fading interference as the distance between coherent states decreases.

The photon-number distribution for the QTS is an oscillatory function that is modulated by two Poissonian peaks. This modulation is primarily a QDS effect explained by interference in phase space, but the oscillation between peaks is a QTS effect. The minima and maxima of the photon-number distribution envelope do not shift, as evidenced by the expression for the derivative of the photon-number distribution.

We have discussed a physical implementation of each QTS by obtaining the GS of a quadruple-Gaussian-well potential. Our numerical analysis shows excellent agreement between the QTS and the GS with respect to where the Gaussian peaks and interference effects appear in phase space and how they

look. Some differences arise due to the Gaussian well not corresponding perfectly to parabolic wells.

VI. CONCLUSION

To conclude, the QTS was introduced to extend the idea of so-called Schrödinger cat states by effectively splitting each of the two coherent states in the superposition into two, thereby obtaining the QTS as a superposition of four coherent states. We have calculated and plotted the Wigner functions, marginal distributions, and photon-number distributions and explained the salient features, which appear complicated but can be understood in terms of linear superpositions and beat patterns.

Different cases were presented corresponding to a macroscopically separated superposition of Schrödinger kitten states, a microscopically separated superposition of Schrödinger cat states, and a four-tooth version of the quantum comb state (in the infinite limit) [29]. The features have been explained, and the comb-state analysis could be especially useful as these features are meaningful in experimental efforts towards quantum information processing in a harmonic oscillator. We have shown promising directions for realization of a QTS in superconducting circuits and Bose-Einstein condensates.

Another important aspect of our work is the connection between the QTS and the quadruple-well potential. We solve for Gaussian wells, but of course other wells are possible. Multiple potential wells provide a promising avenue for guiding laboratory realizations of the QTS.

ACKNOWLEDGMENTS

N.S. acknowledges the University of Calgary Eyes High Postdoctoral program. N.A. acknowledges the China Scholarship Council (Grant No. 2016GXYN31). B.C.S. acknowledges NSERC and NSFC (Grant No. 11675164) for financial support.

[1] E. Schrödinger, Der stetige übergang von der mikrozur makromechanik, Sci. Nat. **14**, 664 (1926).
[2] E. Schrödinger, Die gegenwärtige situation in der quantenmechanik, Sci. Nat. **23**, 807 (1935).
[3] K. Husimi, Some formal properties of the density matrix, Proc. Phys. Math. Soc. Jpn. **22**, 264 (1940).
[4] G. J. Milburn, Quantum and classical Liouville dynamics of the anharmonic oscillator, Phys. Rev. A **33**, 674 (1986).
[5] B. Yurke and D. Stoler, Generating Quantum Mechanical Superpositions of Macroscopically Distinguishable States via Amplitude Dispersion, Phys. Rev. Lett. **57**, 13 (1986).
[6] E. Wigner, On the quantum correction for thermodynamic equilibrium, Phys. Rev. **40**, 749 (1932).
[7] M. Hillery, R. F. O'Connell, M. O. Scully, and E. P. Wigner, Distribution functions in physics: Fundamentals, Phys. Rep. **106**, 121 (1984).
[8] W. P. Schleich, *Quantum Optics in Phase Space* (Wiley-VCH, Weinheim, 2001).
[9] U. Leonhardt, *Essential Quantum Optics: From Quantum Measurements to Black Holes* (Cambridge University Press, New York, 2013).
[10] V. Bužek and P. L. Knight, The origin of squeezing in a superposition of coherent states, Opt. Commun. **81**, 331 (1991).
[11] K. Banaszek and K. Wódkiewicz, Sampling quantum phase space with squeezed states, Opt. Express **3**, 141 (1998).
[12] G. J. Milburn and C. A. Holmes, Dissipative Quantum and Classical Liouville Mechanics of the Anharmonic Oscillator, Phys. Rev. Lett. **56**, 2237 (1986).
[13] R. J. Glauber, Coherent and incoherent states of the radiation field, Phys. Rev. **131**, 2766 (1963).
[14] V. V. Dodonov, I. A. Malkin, and V. I. Man'ko, Even and odd coherent states and excitations of a singular oscillator, Physica **72**, 597 (1974).
[15] B. C. Sanders, Superposition of two squeezed vacuum states and interference effects, Phys. Rev. A **39**, 4284 (1989).
[16] B. C. Sanders, Superpositions of distinct phase states by a nonlinear evolution, Phys. Rev. A **45**, 7746 (1992).
[17] A. Ourjoumtsev, R. Tualle-Brouri, J. Laurat, and P. Grangier, Generating optical Schrödinger kittens for quantum information processing, Science **312**, 83 (2006).
[18] A. Ourjoumtsev, H. Jeong, R. Tualle-Brouri, and P. Grangier, Generation of optical 'Schrödinger cats' from photon number states, Nature (London) **448**, 784 (2007).
[19] B. C. Sanders, Entangled coherent states, Phys. Rev. A **45**, 6811 (1992).
[20] B. C. Sanders, Erratum: Entangled coherent states, Phys. Rev. A **46**, 2966 (1992).
[21] B. C. Sanders, Review of entangled coherent states, J. Phys. A: Math. Theor. **45**, 244002 (2012).
[22] C. Wang, Y. Y. Gao, P. Reinhold, R. W. Heeres, N. Ofek, K. Chou, C. Axline, M. Reagor, J. Blumoff, K. M. Sliwa, L. Frunzio, S. M. Girvin, L. Jiang, M. Mirrahimi, M. H. Devoret, and R. J. Schoelkopf, A Schrödinger cat living in two boxes, Science **352**, 1087 (2016).
[23] C. G. Christopher and G. Rainer, Two-mode SU(2) and SU(2) Schrödinger cat states, J. Mod. Opt. **44**, 41 (1997).
[24] K. Nemoto and B. C. Sanders, Superpositions of SU(3) coherent states via a nonlinear evolution, J. Phys. A: Math. Gen. **34**, 2051 (2001).
[25] V. Bužek, A. Vidiella-Barranco, and P. L. Knight, Superpositions of coherent states: Squeezing and dissipation, Phys. Rev. A **45**, 6570 (1992).
[26] A. Miranowicz, R. Tanas, and S. Kielich, Generation of discrete superpositions of coherent states in the anharmonic oscillator model, Quantum Opt. **2**, 253 (1990).
[27] J. Janszky, P. Domokos, and P. Adam, Coherent states on a circle and quantum interference, Phys. Rev. A **48**, 2213 (1993).
[28] C. W. Gardiner, *Handbook of Stochastic Methods: For Physics, Chemistry and Natural Sciences*, 2nd ed., Springer Series in Synergetics Vol. 13 (Springer, Berlin, 1985).
[29] D. Gottesman, A. Kitaev, and J. Preskill, Encoding a qubit in an oscillator, Phys. Rev. A **64**, 012310 (2001).

[30] S. Ghose and B. C. Sanders, Non-Gaussian ancilla states for continuous variable quantum computation via Gaussian maps, J. Mod. Opt. **54**, 855 (2007).
[31] C. Flühmann, T. L. Nguyen, M. Marinelli, V. Negnevitsky, K. Mehta, and J. P. Home, Encoding a qubit in a trapped-ion mechanical oscillator, Nature **566**, 513 (2019).
[32] P. Adam, J. Janszky, and A. V. Vinogradov, Amplitude squeezed and number-phase intelligent states via coherent state superposition, Phys. Lett. A **160**, 506 (1991).
[33] J. Janszky and An. V. Vinogradov, Squeezing via One-Dimensional Distribution of Coherent States, Phys. Rev. Lett. **64**, 2771 (1990).
[34] W. H. Zurek, Sub-Planck structure in phase space and its relevance for quantum decoherence, Nature (London) **412**, 712 (2001).
[35] K. Vogel and H. Risken, Determination of quasiprobability distributions in terms of probability distributions for the rotated quadrature phase, Phys. Rev. A **40**, 2847 (1989).
[36] N. Delfosse, P. Allard Guerin, J. Bian, and R. Raussendorf, Wigner Function Negativity and Contextuality in Quantum Computation on Rebits, Phys. Rev. X **5**, 021003 (2015).
[37] J. H. Shapiro, H. Yuen, and A. Mata, Optical communication with two-photon coherent states—Part II: Photoemissive detection and structured receiver performance, IEEE Trans. Inf. Theory **25**, 179 (1979).
[38] H. Yuen and J. H. Shapiro, Optical communication with two-photon coherent states—Part III: Quantum measurements realizable with photoemissive detectors, IEEE Trans. Inf. Theory **26**, 78 (1980).
[39] T. Tyc and B. C. Sanders, Operational formulation of homodyne detection, J. Phys. A: Math. Gen. **37**, 7341 (2004).
[40] W. P. Schleich and J. A. Wheeler, Oscillations in photon distribution of squeezed states and interference in phase space, Nature (London) **326**, 574 (1987).
[41] V. Bužek, M. S. Kim, and T. Gantsog, Quantum phase distributions of amplified Schrödinger-cat states of light, Phys. Rev. A **48**, 3394 (1993).
[42] W. P. Schleich, M. Pernigo, and F. L. Kien, Nonclassical state from two pseudoclassical states, Phys. Rev. A **44**, 2172 (1991).
[43] N. A. Ansari and V. I. Manko, Photon statistics of multimode even and odd coherent light, Phys. Rev. A **50**, 1942 (1994).
[44] V. V. Dodonov, V. I. Manko, and D. E. Nikonov, Even and odd coherent states for multimode parametric systems, Phys. Rev. A **51**, 3328 (1995).
[45] A. O. Caldeira and A. J. Leggett, Quantum tunneling in a dissipative system, Ann. Phys. (NY) **149**, 374 (1983).
[46] M. J. Steel and M. J. Collett, Quantum state of two trapped Bose-Einstein condensates with a Josephson coupling, Phys. Rev. A **57**, 2920 (1998).
[47] J. I. Cirac, M. Lewenstein, K. Mølmer, and P. Zoller, Quantum superposition states of Bose-Einstein condensates, Phys. Rev. A **57**, 1208 (1998).
[48] J. Ruostekoski, *Directions in Quantum Optics* (Springer, Berlin, 2001).
[49] T. J. Haigh, A. J. Ferris, and M. K. Olsen, Demonstrating mesoscopic superpositions in double-well Bose-Einstein condensates, Opt. Commun. **283**, 3540 (2010).
[50] S.-l. Ma, J.-k. Xie, and F.-l. Li, Generation of superposition coherent states of microwave fields via dissipation of a superconducting qubit with broken inversion symmetry, Phys. Rev. A **99**, 022302 (2019).
[51] E. C. G. Sudarshan, Equivalence of Semiclassical and Quantum Mechanical Descriptions of Statistical Light Beams, Phys. Rev. Lett. **10**, 277 (1963).
[52] K. E. Cahill and R. J. Glauber, Ordered expansions in boson amplitude operators, Phys. Rev. **177**, 1857 (1969).
[53] A. Gilchrist, K. Nemoto, W. J. Munro, T. C. Ralph, S. Glancy, S. L. Braunstein, and G. J. Milburn, Schrödinger cats and their power for quantum information processing, J. Opt. B **6**, S828 (2004).
[54] A. Mecozzi and P. Tombesi, Distinguishable Quantum States Generated via Nonlinear Birefringence, Phys. Rev. Lett. **58**, 1055 (1987).
[55] M. Brune, S. Haroche, J. M. Raimond, L. Davidovich, and N. Zagury, Manipulation of photons in a cavity by dispersive atom-field coupling: Quantum-nondemolition measurements and generation of "Schrödinger cat" states, Phys. Rev. A **45**, 5193 (1992).
[56] C.-W. Lee, J. Lee, H. Nha, and H. Jeong, Generating a Schrödinger-cat-like state via a coherent superposition of photonic operations, Phys. Rev. A **85**, 063815 (2012).
[57] C. M. Savage, S. L. Braunstein, and D. F. Walls, Macroscopic quantum superpositions by means of single-atom dispersion, Opt. Lett. **15**, 628 (1990).
[58] A. P. Lund, H. Jeong, T. C. Ralph, and M. S. Kim, Conditional production of superpositions of coherent states with inefficient photon detection, Phys. Rev. A **70**, 020101(R) (2004).
[59] M. Dakna, T. Anhut, T. Opatrný, L. Knöll, and D.-G. Welsch, Generating Schrödinger-cat-like states by means of conditional measurements on a beam splitter, Phys. Rev. A **55**, 3184 (1997).
[60] A. J. Leggett, Macroscopic quantum systems and the quantum theory of measurement, Prog. Theor. Phys. Suppl. **69**, 80 (1980).
[61] C. Monroe, D. M. Meekhof, B. E. King, and D. J. Wineland, A "Schrödinger cat" superposition state of an atom, Science **272**, 1131 (1996).
[62] K. G. Johnson, J. D. Wong-Campos, B. Neyenhuis, J. Mizrahi, and C. Monroe, Ultrafast creation of large Schrödinger cat states of an atom, Nat. Commun. **8**, 697 (2017).
[63] D. Kienzler, C. Flühmann, V. Negnevitsky, H.-Y. Lo, M. Marinelli, D. Nadlinger, and J. P. Home, Observation of Quantum Interference between Separated Mechanical Oscillator Wave Packets, Phys. Rev. Lett. **116**, 140402 (2016).
[64] C. Flühmann, V. Negnevitsky, M. Marinelli, and J. P. Home, Sequential Modular Position and Momentum Measurements of a Trapped Ion Mechanical Oscillator, Phys. Rev. X **8**, 021001 (2018).
[65] J.-Q. Liao, J.-F. Huang, and L. Tian, Generation of macroscopic Schrödinger-cat states in qubit-oscillator systems, Phys. Rev. A **93**, 033853 (2016).
[66] M. Sasaki, M. Takeoka, and H. Takahashi, Temporally multiplexed superposition states of continuous variables, Phys. Rev. A **77**, 063840 (2008).
[67] T. Gerrits, S. Glancy, T. S. Clement, B. Calkins, A. E. Lita, A. J. Miller, A. L. Migdall, S. W. Nam, R. P. Mirin, and E. Knill, Generation of optical coherent-state superpositions by number-resolved photon subtraction from the squeezed vacuum, Phys. Rev. A **82**, 031802(R) (2010).

[68] J. S. Neergaard-Nielsen, B. M. Nielsen, C. Hettich, K. Mølmer, and E. S. Polzik, Generation of a Superposition of Odd Photon Number States for Quantum Information Networks, Phys. Rev. Lett. **97**, 083604 (2006).

[69] W. Asavanant, K. Nakashima, Y. Shiozawa, J.-I. Yoshikawa, and A. Furusawa, Generation of highly pure Schrödinger's cat states and real-time quadrature measurements via optical filtering, Opt. Express **25**, 32227 (2017).

[70] H. Takahashi, K. Wakui, S. Suzuki, M. Takeoka, K. Hayasaka, A. Furusawa, and M. Sasaki, Generation of Large-Amplitude Coherent-State Superposition via Ancilla-Assisted Photon Subtraction, Phys. Rev. Lett. **101**, 233605 (2008).

[71] J. Etesse, M. Bouillard, B. Kanseri, and R. Tualle-Brouri, Experimental Generation of Squeezed Cat States with an Operation Allowing Iterative Growth, Phys. Rev. Lett. **114**, 193602 (2015).

[72] A. Ourjoumtsev, F. Ferreyrol, R. Tualle-Brouri, and P. Grangier, Preparation of non-local superpositions of quasi-classical light states, Nat. Phys. **5**, 189 (2009).

[73] B. Vlastakis, G. Kirchmair, Z. Leghtas, S. E. Nigg, L. Frunzio, S. M. Girvin, M. Mirrahimi, M. H. Devoret, and R. J. Schoelkopf, Deterministically encoding quantum information using 100-photon Schrödinger cat states, Science **342**, 607 (2013).

[74] S. Ding, G. Maslennikov, R. Hablützel, H. Loh, and D. Matsukevich, Quantum Parametric Oscillator with Trapped Ions, Phys. Rev. Lett. **119**, 150404 (2017).

[75] S. Haroche, Nobel lecture: Controlling photons in a box and exploring the quantum to classical boundary, Rev. Mod. Phys. **85**, 1083 (2013).

[76] L. I. Schiff, *Quantum Mechanics*, 3rd ed. (McGraw-Hill, New York, 1968), pp. 61–62.

[77] S. Nandi, Quantum Gaussian wells and barriers, Am. J. Phys. **79**, 752 (2011).